# Competition between Two Forms of Ordering in Finite Coulomb Clusters

Hiroo Totsuji,* Tokunari Kishimoto, Chieko Totsuji, and Kenji Tsuruta

*Graduate School of Natural Science and Technology and Faculty of Engineering, Okayama University, Tsushimanaka 3-1-1, Okayama 700-8530, Japan*

(Received 2 October 2001; published 7 March 2002)

The lowest-energy state of spherical clusters made up of single-species charged particles in a three-dimensional confining potential is investigated by molecular dynamics simulations for a system size of $5 \times 10^3$ to $1.2 \times 10^5$. The energy per particle is compared between shell-structured clusters and spherical finite-bcc lattices with relaxed surfaces. The shell structure in the interior is the lowest-energy configuration for ion numbers lower than about $10^4$, while for higher ion numbers, an interior with bcc ordering surrounded by a few shells on the outside has lower energy. The formation of a small bcc lattice (nucleation) in the shell-structured cluster of $2 \times 10^4$ ions is observed.

DOI: 10.1103/PhysRevLett.88.125002 PACS numbers: 52.27.Jt, 52.27.Gr, 52.65.Yy, 61.46.+w

Large clusters of laser-cooled ions confined in the Penning-Malmberg and the Paul traps have provided us with clear examples of the strongly coupled plasma [1–6]. One of the most remarkable phenomena observed is the crystallization of ions of one species induced by their mutual repulsive Coulomb interaction. Since the effect of traps is equivalent to the existence of the uniform neutralizing background charge and the body-centered cubic (bcc) lattice is the lowest-energy state of the (infinite) one-component plasma (OCP) [7], one may expect to find bcc ordering in the interior of clusters sufficiently large, such that the influence of the geometry of confinement and the surface is overcome. The critical cluster size where the bulk form of ordering appears in the interior may be compared to the value on the order of $10^3$, for systems such as clusters of inert-gas atoms, where the force has shorter range [8].

In experiments, a bcc form of ordering has been observed in the interior of ion clusters containing more than a few times $10^5$ ions [9,10]. For smaller clusters, shell structure has been seen for the entire volume, with the shells parallel to the outer surface, which is defined by the geometry of confinement [4]. The transition to bcc order in the interior has been estimated (from one-dimensional calculations) to occur in systems with more than about $10^5$ ions [1]. Numerical simulations can give a more precise description on such a transition, but the largest system for which simulations have been reported was for $2 \times 10^4$ ions, which showed no bcc order in the interior [11]. The purpose of this Letter is to study this behavior for ion numbers in the range of $5 \times 10^3$ to $1.2 \times 10^5$.

We consider the one-component plasma confined by the spherically symmetric parabolic potential. The parabolic form is common for all ion traps and, though the spherical symmetry is assumed for simplicity, the results will also apply to spheroidal clusters with small modifications. The Hamiltonian is $K + U$ with the kinetic energy $K$ and the potential energy $U$, which we rewrite as

$$U = \sum_{i>j}^{N} \frac{q^2}{|\mathbf{r}_i - \mathbf{r}_j|} + \sum_{i=1}^{N} \frac{k\mathbf{r}_i^2}{2} = \frac{q^2}{a}\left[\sum_{i>j}^{N} \frac{1}{|\mathbf{r}_i' - \mathbf{r}_j'|} + \sum_{i=1}^{N} \frac{(\mathbf{r}_i')^2}{2}\right], \quad (1)$$

giving all distances in units of the Wigner-Seitz radius $a$ defined by $a = (q^2/k)^{1/3}$.

When charges are regarded as continuum (the fluid approximation), the lowest-energy state is the homogeneous distribution up to the radius $R = (Nq^2/k)^{1/3} = N^{1/3}a$ with the density $n = (3/4\pi)(k/q^2) = (3/4\pi)a^3$ and $U = U_{\text{homo}} = (9/10)N^{5/3}(q^2/a)$ ($a$ is the mean distance or the ion-sphere radius in this approximation). For given configurations, we define the cohesive (correlation or Madelung) energy per particle by $u_{\text{coh}} = (U - U_{\text{homo}})/(Nq^2/a)$ and compare $u_{\text{coh}}$ for various structures. When $N = \infty$, $u_{\text{coh}}$ reduces to the values for OCP [7].

At zero temperature, the behavior of the system is determined by $U$ and (1) indicates that our system is characterized only by $N$. At finite temperatures $T$, we define the dimensionless parameter $\Gamma = q^2/k_B T a$ and static properties are characterized by $N$ and $\Gamma$.

In the fluid approximation, the radius of uniform distribution oscillates with the frequency $\omega_p = (3k/m)^{1/2} = (4\pi q^2 n/m)^{1/2}$. The time $2\pi/\omega_p$ characterizes the macroscopic evolution of our system. One of the microscopic characteristic time scales may be the time to traverse $a$ by thermal velocity $a/(k_B T/m)^{1/2} = (3\Gamma)^{1/2}(2\pi/\omega_p)$.

We perform molecular dynamics simulations employing the $O(N)$ fast multipole method (FMM) [12]. We recursively divide the system into small cells and compute the contributions to force the potential from well-separated cells by the multipole and Taylor expansions, applying direct computation only to those from nearby cells [13]. The cohesive energy given by FMM is slightly larger than the exact value obtained by direct computation; $u_{\text{coh}}^{\text{FMM}} = u_{\text{coh}} + \Delta$, where $\Delta(>0)$ is not sensitive to configuration

 © 2002 The American Physical Society 

and $\Delta \sim (7 \pm 1) \times 10^{-5}$ for $N \sim 10^5$. We follow the dynamics using FMM, monitoring $u_{\rm coh}$ through $u_{\rm coh}^{\rm FMM}$ with the ambiguity of $\pm 1$ in the fifth digit, and directly compute $u_{\rm coh}$ for final relaxed states. The temperature is controlled by the Nosé-Hoover thermostats [14]. In order to keep the homogeneity of the temperature, we attach multiple thermostats each controlling about 5000 particles at the same temperature. We anneal the system for a sufficiently long time, $3 \times 10^2(2\pi/\omega_p)$ for $N \sim 10^5$ and longer for smaller systems, and cool the system slowly enough, reducing the temperature stepwise typically by 10%. The cooling time scale $\tau = \Gamma/\dot{\Gamma}$ is taken to be sufficiently longer than that of relaxation for the potential and kinetic energies at each specified temperature: $\tau > 6 \times 10^2(2\pi/\omega_p)$ for $\Gamma < 300$ and $\tau \sim (2\text{–}10) \times 10^2(2\pi/\omega_p)$ otherwise, total duration and final values of $\Gamma$ being more than $1.2 \times 10^3(2\pi/\omega_p)$ and more than $10^5$, respectively. These time scales are much longer than $2\pi/\omega_p$ and $2\pi(3\Gamma)^{1/2}/\omega_p$.

We start from two kinds of initial conditions: (i) the uniform random distribution of particles within the sphere of the radius $R$ and (ii) the spherical cutout of the bcc lattice (spherical bcc matter). In both cases, initial velocities are given by the random distribution corresponding to the temperature specified by $\Gamma$. These two sets of initial conditions lead to different final zero-temperature states when the temperature is slowly lowered. The former gives shell-structured clusters while the latter gives finite bcc lattices with reconstructed surfaces.

When we start from the initial condition (i), we first anneal the system at the temperature above the melting point of OCP (with typical values of $\Gamma$ around 100) and then slowly cool the system. With the decrease of the temperature, the formation of spherical shells advances from the periphery to the center. The system sizes of our simulations are $N = 5000$, $10^4$, 20 288, and $10^5$ and Figs. 1 and 2 show the radial distribution functions and slices including the center of the sphere in the final state of some examples. Outer shells are clear and well defined, the radial distribution function hitting zero between them. The sharpness of shells decreases with the decrease of the distance from the center. However, we still have shells near the center though they are diffuse and cannot be decomposed completely.

For a given $N$, the final configuration depends on the history of cooling and the initial conditions [within (i)]. To check this dependency, we have followed two examples for $N = 5000$ and $10^4$ and in other cases, repeated annealing and cooling. After sufficiently slow cooling, the radial distribution is very similar especially for the outer part. The cohesive energy is also similar and the difference in the fourth leading digit seems to be less than 2: The cohesion usually becomes stronger by repeated annealing but once cooled down sufficiently slowly, the cohesive energy does not change to such an extent. This may indicate that there exist many local minima of the total potential energy with similar values for the shell-structured configurations.

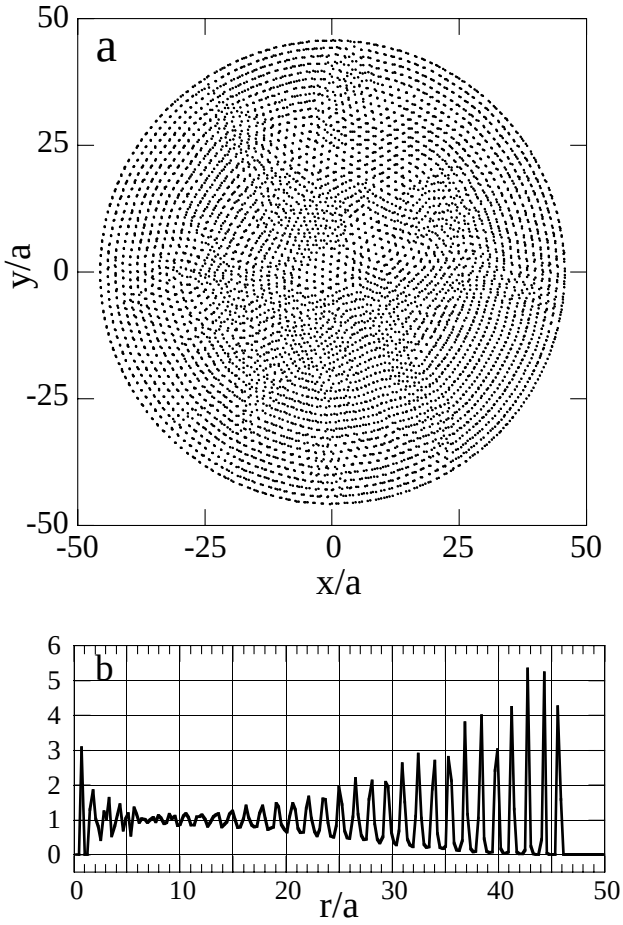


FIG. 1. Shell-structured cluster of $10^5$ charges. Configuration near the equatorial plane with $|z| < 2.06a$ (a) and radial distribution normalized by average density (b).

The values of the cohesive energy of the shell-structured spherical systems are shown in Table I and plotted in Fig. 3. These values can be interpolated as

$$u_{\rm coh} = -0.895\,03 + 0.0401N^{-1/3} \qquad (2)$$

for $5000 < N < 10^5$ (with coefficients effective up to the fifth digit in $u_{\rm coh}$). We note that the cohesive energy of shell-structured states is not expected to have well-defined asymptotic behavior; when $N \to \infty$, shell structures may even lose the stability as a local minima of the total potential energy. For our purpose, it is therefore necessary to have the values of cohesive energy for large clusters instead of extrapolating from those of smaller clusters.

In the initial state (ii), the spherical bcc matter has rather high surface energy [1,15]. The initial cohesive energy depends on the position of the center of the potential well relative to lattice points. Starting from (ii), we anneal the system keeping the temperature near but below the melting point. We then lower the temperature slowly and obtain the finite spherical bcc lattice with reconstructed surface. The system sizes of our simulations are $N =$ 4544, 10 464, 20 288, 48 928, and 120 032. An example of the structures is shown in Fig. 4. We observe that the

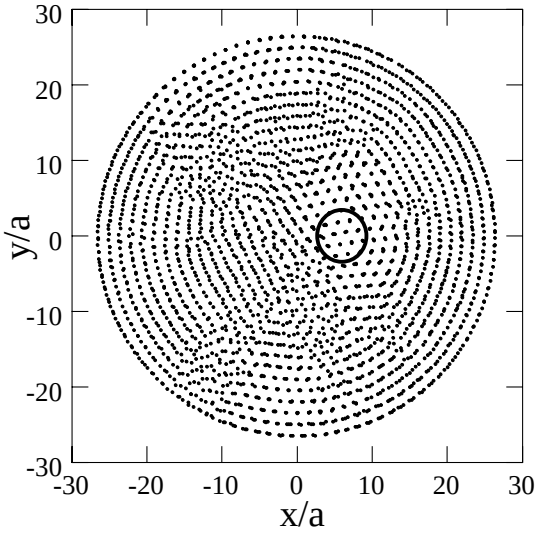


FIG. 2. The same as Fig. 1a for the shell-structured cluster of 20 288 charges. Configuration is shown for particles with $|z| < 2.42a$. (As for the circle, see Fig. 5.)

relaxation has occurred only within a few layers at the surface. The cohesive energy of the spherical bcc matter with reconstructed surface is shown in Table I and plotted in Fig. 3. The relaxation near the surface largely enhances the cohesion [15]. This has not been expected from the weak cohesion of unrelaxed spherical bcc matter.

When we anneal the spherical bcc matter at higher temperatures, the reconstruction of the surface advances inward further. The resultant cohesion of the system, however, becomes weaker. Thus the final states obtained above are local minima which are reached starting from the spherical bcc matter.

In the limit of very large values of $N$, the cohesive energy of the spherical bcc matter with a reconstructed surface may have the form

$$u_{\mathrm{coh}} = E_\infty + E_s N^{-1/3}, \tag{3}$$

where $E_\infty = -0.895\,929$ (the Madelung energy of the bcc lattice) and the second term expresses the effect of the surface. When fitted to this form as shown in Fig. 3 by the solid line, we have $E_s = 0.0598$.

The zero-temperature cohesive energies of the shell-structured clusters and of finite bcc matters with relaxed surface are compared in Fig. 3. We observe that, when the system size exceeds the critical value $N_c$, stronger cohesion is given by finite bcc lattices with relaxed surfaces rather than shell-structured clusters. The critical system size is estimated from (2) and (3) as $N_c = 1.05 \times 10^4$. We here note that the cohesive energy, especially of shell structures, could become lower by annealing the system repeatedly. When we estimate the latter effect by changing the fourth digit of the cohesive energy of shell structures by unity, we have

$$1.1 \times 10^4 < N_c < 1.5 \times 10^4. \tag{4}$$

The critical size $N_c$ may also be defined for transitions at low but finite temperatures. Though $N_c$ does not seem to depend on the temperature when $\Gamma$ is larger than a few hundreds, the temperature effect has not been explored.

In experiments, the shell and the bcc structures have been observed in clusters of $1.5 \times 10^4$ and $2 \times 10^5$ ions, respectively [4,10]. The critical size, however, has not been determined. We note that the shell-structured cluster is still a metastable state at a local minimum of the total potential energy in the domain $N > N_c$. Therefore it is not strange that the shell-structured clusters with $N > N_c$ do not evolve into bcc lattices with relaxed surfaces in our simulations. The system has to overcome the barrier of the total potential energy in order to relax to a lower energy state and, once the system is in the state of higher potential energy, it takes a very long time for the main part of the system to be organized into lattices. In addition to this, clusters of ions are rotating in experiments, and any effects which disturb the solid rotation, such as collisions with residual atoms and molecules, may keep the system from being organized into lattices as a whole. Thus a little larger critical value might be obtained in experiments starting from random configurations.

As discussed above, it is not expected that shell structures go under the structural transition in the process of cooling even when $N > N_c$. One may, however, expect

TABLE I. Cohesive energy of shell-structured clusters and finite bcc lattices with relaxed surfaces. When we have two examples, ambiguity in the fifth digit is estimated and shown in ( ).

| Shell-structured cluster | | bcc with relaxed surface | |
|---|---|---|---|
| $N$ | $u_{\mathrm{coh}}$ | N | $u_{\mathrm{coh}}$ |
| 5000 | −0.892 68(6) | 4544 | −0.892 32 |
| 10 000 | −0.893 15(1) | 10 464 | −0.893 35 |
| 20 288 | −0.893 59 | 20 288 | −0.893 75 |
| 100 000 | −0.894 15 | 48 928 | −0.894 10 |
| | | 120 032 | −0.894 60 |

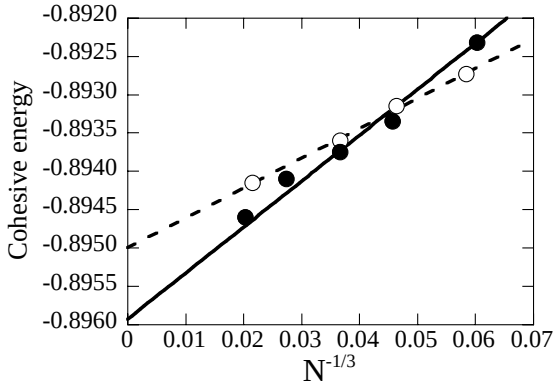


FIG. 3. Cohesive energy per particle of spherical Coulomb clusters. Open and filled circles are shell-structured clusters and finite bcc lattices with relaxed surfaces, respectively, and broken and solid lines are interpolations.

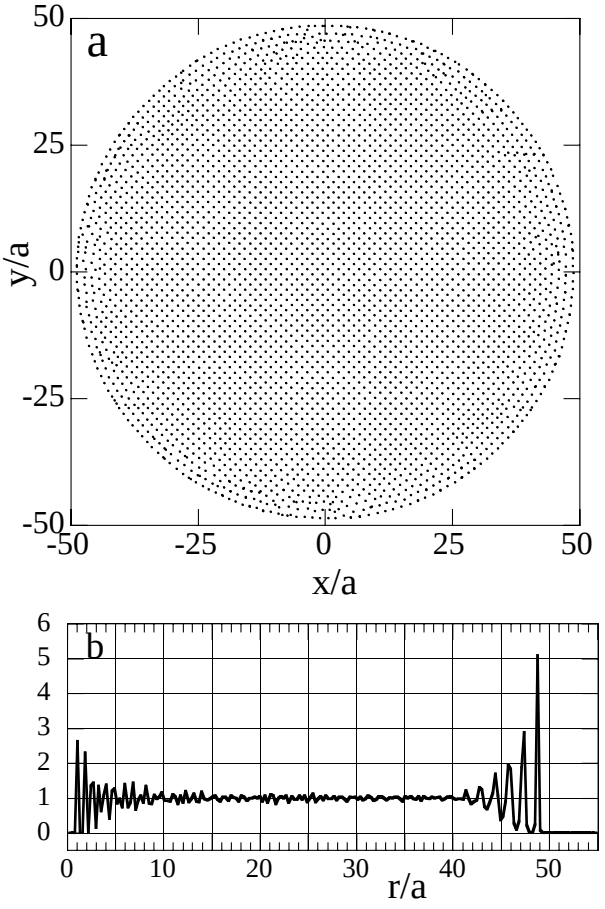


FIG. 4. The same as Fig. 1 for a finite bcc lattice of 120 032 charges with reconstructed surface. Configuration (a) is shown for particles with $|z| < 2.19a$.

that there is a chance for small bcc lattices to develop in the clusters of larger sizes.

In Fig. 2, there exists a domain where we have a regular straight structure rather than planes curved in accordance with the surface. The structure factor for 48 particles included in a sphere centered in this domain is shown in Fig. 5. We clearly see that the Bragg spots forms the fcc structure in the wave-number space. We have confirmed that the spacing between Bragg spots is consistent with the bcc lattice with the average density of this cluster within a few percent. This domain thus forms the bcc lattice nucleated from the shell-structured cluster.

To summarize, it is shown that finite bcc lattices with relaxed surfaces have stronger cohesion relative to shell-structured clusters when the system size exceeds about $10^4$ in the low-temperature limit. In the shell-structured cluster of $2 \times 10^4$, the nucleation of the bcc lattice is observed.

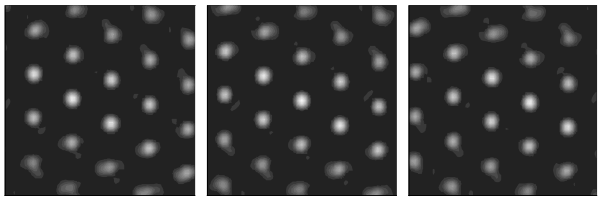

FIG. 5. Bragg patterns from particles in the central part of the shell-structured cluster of 20 288 charges: The particles are in a sphere centered at $(6.06, 0, 0)a$ shown by the solid line in Fig. 2. These planes, $\mathbf{k} \cdot \mathbf{n}/(2\pi/a) = -0.569, 0, 0.569$ (from left to right), $\mathbf{n} = (-0.0764, -0.0643, 0.995)$, form three successive close packed (111) planes in the fcc lattice.

This work has been partly supported by the Grant-in-Aid for Scientific Research (B) from the Ministry of Education, Culture, Sports, Science and Technology of Japan, No. 08458109 and No. 11480110.

*Email address: totsuji@elec.okayama-u.ac.jp

[1] For a review, see D. H. E. Dubin and T. M. O'Neil, Rev. Mod. Phys. **71**, 87 (1999).
[2] A. Rahman and J. P. Schiffer, Phys. Rev. Lett. **57**, 1133 (1986).
[3] D. H. E. Dubin and T. M. O'Neil, Phys. Rev. Lett. **60**, 511 (1988).
[4] S. L. Gilbert, J. J. Bollinger, and D. J. Wineland, Phys. Rev. Lett. **60**, 2022 (1988).
[5] G. Birkl, S. Kassner, and H. Walther, Nature (London) **357**, 310 (1992).
[6] M. Drewsen, C. Brodersen, and L. Hornekær, J. S. Hangst, and J. P. Schiffer, Phys. Rev. Lett. **81**, 2878 (1998).
[7] S. G. Brush, H. L. Sahlin, and E. Teller, J. Chem. Phys. **45**, 2102 (1966).
[8] For example, see J. W. Lee and G. D. Stein, J. Phys. Chem. **91**, 2450 (1987).
[9] W. M. Itano, J. J. Bollinger, J. N. Tan, B. Jelenković, X.-P. Huang, and D. J. Wineland, Science **279**, 686 (1998).
[10] J. J. Bollinger, T. B. Mitchell, X.-P. Huang, W. M. Itano, J. N. Tan, B. Jelenković, and D. J. Wineland, Phys. Plasmas **7**, 7 (2000).
[11] J. P. Schiffer, *Non-Neutral Plasma Physics II*, edited by J. Fajans and D. H. E. Dubin, AIP Conf. Proc. No. 331 (AIP, New York, 1995), p. 191.
[12] L. Greengard and V. Rokhlin, J. Comput. Phys. **73**, 325 (1987).
[13] For $N \sim 10^5$, we adopt level 5, multipole expansion up to $2^6$th order, Taylor expansion up to 6th order, and well separatedness 2. Similar or better accuracy is kept for smaller systems.
[14] S. Nosé, J. Chem. Phys. **81**, 511 (1984).
[15] T. Kishimoto, C. Totsuji, K. Tsuruta, and H. Totsuji, Phys. Lett. A **281**, 256 (2001).